Journal of Hydrology xxx (xxxx) xxx

Contents lists available at ScienceDirect

Journal of Hydrology

journal homepage: www.elsevier.com/locate/jhydrol

Research papers

Probabilistic identification of Preferential Groundwater Networks

Massimiliano Schiavo [a,*], Monica Riva [a,b,*], Laura Guadagnini [c], Erwin Zehe [d], Alberto Guadagnini [a,b]

[a] Dipartimento di Ingegneria Civile e Ambientale, Politecnico di Milano, Piazza L. Da Vinci 32, 20133 Milano, Italy
[b] Department of Hydrology and Atmospheric Sciences, The University of Arizona, Tucson, AZ 85721, USA
[c] Department of Civil and Environmental Engineering, Universitat Politècnica de Catalunya, Jordi Girona 1-3, 08034 Barcelona, Spain
[d] Karlsruhe Institute of Technology, Institute of Water and River Basin Management, Karlsruhe, Germany

ARTICLE INFO

Keywords:
Preferential Groundwater Networks
Monte Carlo simulations
Minimum energy expenditure
Probabilistic approaches
Geostatistics

ABSTRACT

We characterize key features of subsurface flow paths relying on an energetic and probabilistic perspective. We consider subsurface flow in a free aquifer system as mainly ruled by gravity, the latter acting as the key driving force. Therefore, we study groundwater circulation relying upon stochastic simulations of aquifer bottom topography inferred from stratigraphic observations. Upon resting on the concept of optimal channel networks, we identify *Preferential Groundwater Networks* (PGNs) as spatially organized structures carved by locally following the steepest gradient associated with the aquifer bottom topography. A probabilistic description of PGNs is obtained by reconstructing the aquifer bottom topography as a spatial random field conditional on the available information, and using diverse area threshold values for PGNs delineation. We find that PGNs inferred from the (ensemble) averaged bottom topography with the highest area threshold considered are strikingly consistent with main flow directions and key subsurface flow patterns inferred from available piezometric data. The probabilistic distribution of PGNs is also consistent with geological and hydrogeological information at our disposal, such as geological data (and ensuing hydrogeological sections), and is coherent with the nature of the aquifers investigated.

1. Introduction

Delineation of main subsurface flow directions within complex hydrogeological systems is relevant to a variety of engineering and environmental scenarios. We address this challenging issue through a slope-driven phenomenological interpretation of subsurface flow. We do so upon leveraging on some of the key concepts developed for surface hydrology and ground our analysis on energy extremal principles (e.g., Banavar et al., 2000; Rodriguez-Iturbe et al., 1992; Rinaldo et al., 2006; Hergarten et al., 2014) to set-up a stochastic framework for the demarcation of preferential pathways across a subsurface aquifer system in the presence of scarce hydrogeological information.

One of the earliest thermodynamic perspectives on landscape evolution was proposed by Leopold and Langbein (1962). These authors illustrated the concept of entropy as a driver to landscape evolution. They relied on the depiction of a river system through a thermodynamic engine model and considered the principle of least work (or, equivalently, constant entropy production per flow volume) to show that the most likely profile of (potential) energy distribution along the entire channel extent can be represented through an exponential functional format. Yang (1976) extended this concept and termed it *minimum stream power*. Howard (1971) proposed that river junctions form angles that are arranged in such a way that they minimize stream power. Howard (1990) expanded this idea by considering that the topology of river networks reflects an energy optimum, a concept that is formulated through a minimization of the total energy dissipation in the network. Rinaldo et al. (1996) and Rodriguez-Iturbe et al. (1992) further contributed to these elements upon postulating that optimal drainage networks minimize overall energy dissipation. These authors relied on the assumption of uniform work per unit flow volume, which in turn implies that the least-demanding energy paths are always identified by the collection of points where local topographic gradients are largest.

In line with these ideas, river networks have been broadly analyzed to extract their tree-like topologies from terrain elevation and energy extremal principles (e.g., Tarboton et al., 1989; Howard, 1990; Tarboton et al., 1991; Tarboton, 1997; Orlandini and Moretti, 2009) and connect

* Corresponding authors at: Dipartimento di Ingegneria Civile e Ambientale, Politecnico di Milano, Piazza L. Da Vinci 32, 20133 Milano, Italy (Monica Riva).
E-mail addresses: massimiliano.schiavo@polimi.it (M. Schiavo), monica.riva@polimi.it (M. Riva).

https://doi.org/10.1016/j.jhydrol.2022.127906
Received 26 October 2021; Received in revised form 27 April 2022; Accepted 29 April 2022
Available online 5 May 2022

these to a statistical description as well as scaling law of synthetic river networks mimicking natural scenarios (Rodriguez-Iturbe et al., 1992; D'Odorico and Rigon, 2003; Reis, 2006). Minimum energy expenditure across a river network implies, in turn, that power (i.e., kinetic energy flux through the network) is maximized. In this context, Kleidon et al. (2013) showed that structural growth in the topology of connected river networks can be characterized through maximization of kinetic energy transfer to transported suspended sediments. Along these lines, Schroers et al. (2021) found evidence that steady state runoff at irrigated hillslopes developed to a maximum power state, where power is equally distributed into sheet and rill flow.

Hergarten et al. (2014) transferred minimum energy dissipation concepts to groundwater systems. They analyzed preferential flow paths that minimize the total energy dissipation associated with a given recharge, under the constraint of an assigned total porosity. Comparing their findings against observations of spring discharge in the Austrian Alps, these authors highlighted some limitations affecting their proposed energy-minimization strategy. The role of bedrock topography in subsurface flow description and quantification was analyzed by Camporese et al. (2019). Berkowitz and Zehe (2020) underlined the need for additional studies to develop a unified theoretical framework comprising surface and subsurface water networks starting from a comprehensive analysis of fractal behaviors and (power-law based) statistical descriptions that are documented for these systems in diverse contexts. Leveraging on energy concepts, Zehe et al. (2021) analyzed fluid flow and solute transport in (synthetically generated) randomly heterogeneous hydraulic conductivity fields and found that high solute concentrations associated with preferential pathways can be correlated with an elevated power in fluid flow therein.

Here, we rely on the concepts illustrated above and mainly developed in the context of surface hydrology and on the idea that seemingly diverse natural phenomena may share similar features. In this context, we identify the probability distribution of preferential subsurface water pathways across an aquifer system (*i*) on the basis of a stochastic reconstruction of aquifer bottom topography conditional on available data, and (*ii*) by making use of energy-minimization concepts. Relying on a stochastic description of the topography of an aquifer bottom is fully consistent with the scarce availability of (geological, sedimentological, and hydrogeological) information. These are typically confined to a limited number of observation boreholes across the subsurface system and are typically tackled in a stochastic context, their associated uncertainty being then propagated onto target quantities of interest (e.g., Bianchi Janetti et al., 2019 and references therein). As a recent example, MacKie et al. (2020) relied on stochastic co-simulations of bedrock elevation and ice-penetrating radar data to assess the way uncertainty in the description of subglacial topography propagates onto a probabilistic description of the routing of water at the glacier bed.

In this framework, we describe the aquifer bottom topography as a random spatial field and model it through a geostatistical framework, which enables us to obtain multiple realizations conditional on available information. These are then embedded in a Monte Carlo framework within which we rely on energy minimization concepts to quantify the spatial distribution (*i*) of subsurface preferential pathways within each system realization and ultimately (*ii*) of the probability that a given location in the domain is associated with a preferential pathway. We recall that, upon assuming that the amount work per unit flow volume along the preferential flow network be uniform, we consider the most probable subsurface paths to be those where local potential energy gradients are maximized, while subsurface flow is spatially self-organized above the aquifer bottom.

Our conceptual framework and operational methodology is then applied in a large-scale subsurface water system located in Italy, upon relying on a set of available geologic-stratigraphic information, to yield a probabilistic description of Preferential Groundwater flow Networks (PGNs). The study is organized as follows. Section 2 describes the field setting and the available data as well as the key elements underpinning the theoretical framework of analysis. Section 3 illustrates the results of the stochastic simulations of PGNs, key conclusions being then drawn in Section 4.

2. Materials and methods

2.1. Field setting and available data

Our study considers a large-scale subsurface water system located in the province of Lecco (Northern Italy) and encompassing a planar extent of approximately 31×25 km^2 (see Fig. 1 for a schematic depiction of the area). It is located in the region delimited at the Eastern and Western boundaries by the two major rivers in the area (i.e., Adda and Lambro, respectively). The current morphology of the area is mainly due to glacial actions which, through deposition and deep excavation of the prequaternary structures, have driven the deposition of moraines, mainly characterizing the northern and central portion of the study area. Subsequently, the action of surface waters remodeled the local relief allowing the formation of river terraces. Limestone formations with some karst patterns, which then degrade toward South into sand and/or gravel formations, can be observed in the northern portion of the system. Major alluvial deposits with clay lenses are a key trait of the southern segment of the region. The main phreatic aquifer is hosted within these sediments. The most productive area is located in the southern region, where the phreatic surface aquifer is characterized by an average thickness of about 35 m (with the largest depth of approximately 95 m below ground level). This aquifer is mainly composed by sand and gravel alluvial geomaterials, with the presence of moraine deposits and rests on a clayey horizon which is mostly continuous in space (Beretta et al., 1984). Groundwater circulation in this free surface alluvial aquifer is characterized by several paleochannels, these being more evident within the Adda river area (Cavallin et al., 1983).

We rely on geologic-stratigraphic information from $N = 222$ boreholes (depicted in Fig. 1). These are employed to identify the elevation $z_n(x, y)$ ($n = 1, 2, \ldots, N$; x and y representing planar coordinates) of the top of the low permeability layer underlying the phreatic aquifer, within which we apply our approach to the identification of PGNs (see Section 2.3). The value of $z_n(x, y)$ assigned at a given borehole location is selected upon assessing that it corresponds to the top of a layer of a clayey or rock geomaterial with a local thickness larger than (or equal to) 1 m. These data are then embedded in a geostatistical analysis framework (see Section 2.2) to yield a collection of (conditional) Monte Carlo (MC) realizations characterizing the level of uncertainty associated with the elevation of the bottom of the free surface aquifer system and hence of the spatial distribution of the PGNs in the region. A total of 8 geologic cross-sections (whose traces are included in Fig. 1) are delineated on the basis of the available stratigraphic information. These are employed to assess the overall consistency of the results obtained with our approach and the general geological setting of the region.

Additional available data used in our study include precipitation records collected between the years 2008 and 2018 at 15 rain gauges (8 of these are comprised in the study area; Fig. 1), land cover information, as well as water levels monitored at surface water bodies (for a total of 5 hydrometric monitoring stations for the Adda and Lambro rivers and the lakes of *Como* and *Pusiano*; see their location in Fig. 1). With reference to available historical piezometric reconstructions, we consider the information that is available (and that is currently employed by local regulators and regional agencies; see *Data Source* Section) as a basis against which we assess the overall consistency of our main results. Average groundwater flow is from North to South (Beretta et al., 1984), the Adda river generally draining water from the aquifer while the Lambro River recharges the aquifer in the northern sector (close to the *Pusiano Lake*; see Fig. 1) and drains it at locations in the southern sector (see also Section 3). Data sources are listed in detail in the *Data Source* Section.

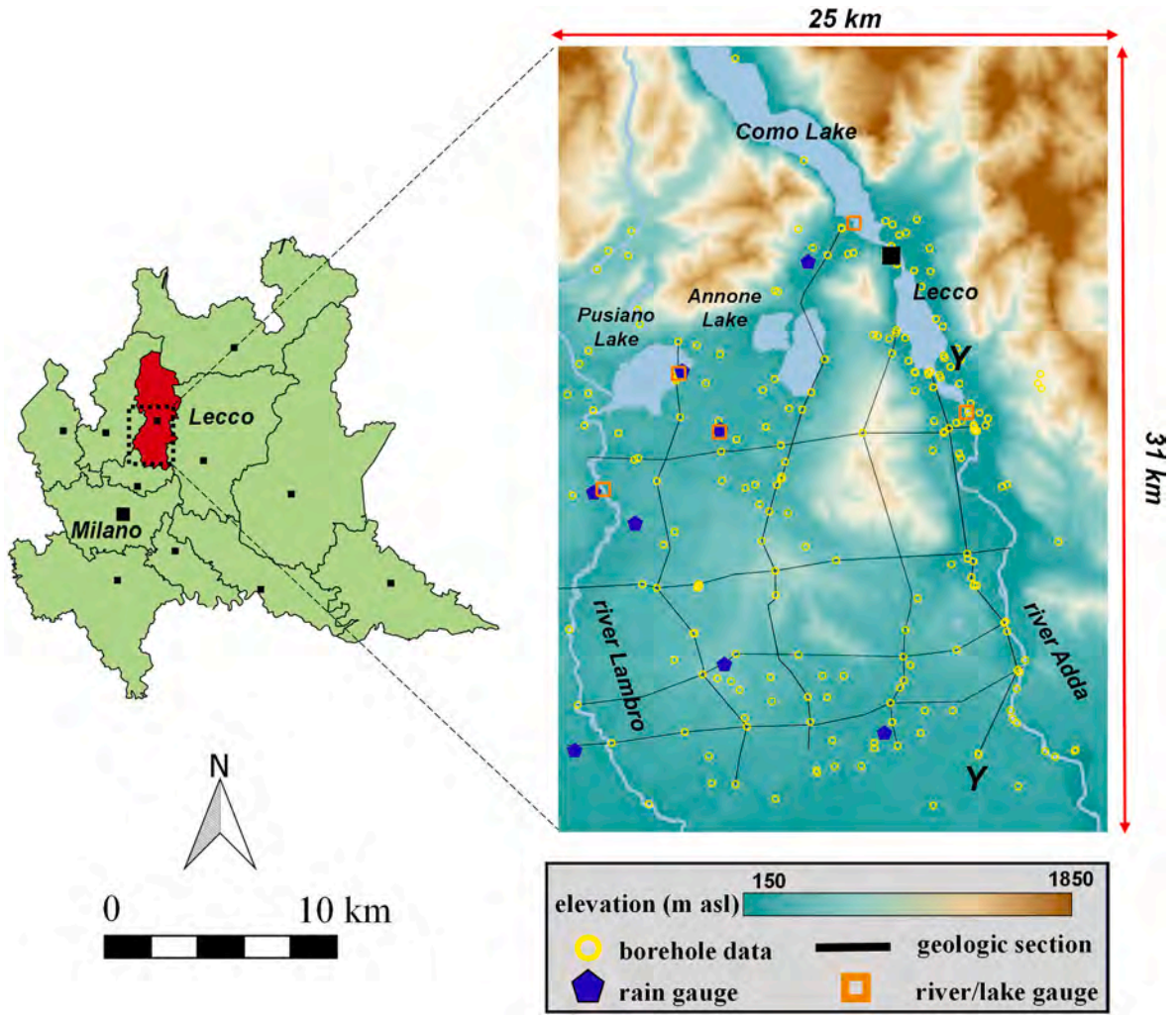

Fig. 1. Sketch of the investigated domain. Locations of available borehole data, rain and river/lake gauges, and traces of geologic sections are also included.

2.2. Conditional simulations of aquifer bottom topography

We start from available borehole data identifying local elevations of the bottom of the free surface aquifer, $z_n(x, y)$, and discretize the domain onto a lattice comprising $m = 77{,}500$ square pixels. Each of the latter is characterized by a side $L = 100$ m and is identified by the coordinate of the centroid, $\mathbf{x}_c = (x_c, y_c)$ ($c = 1, 2, \ldots, m$). We treat the aquifer bottom elevation as a spatial random field and consider an isotropic variogram model to describe its geospatial structure. Variogram parameters are estimated through a Maximum Likelihood (ML) approach (details not shown).

We obtain a collection of *NMC* conditional random realizations of the aquifer bottom topography through the widely known and tested software SGSIM (Deutsch and Journel, 1997). Subsurface gravity-driven flow is then characterized within the context of an energy minimization framework (see Section 2.3) across each of these realizations to include the way an imperfect knowledge of aquifer bottom topography propagates onto the spatial distribution of preferential groundwater flow networks in a field setting.

2.3. Free energy and dissipation in Preferential Groundwater Networks (PGNs)

An energetic perspective on dissipation associated with groundwater flow can be considered upon recalling that due to the first law of thermodynamics the variation in internal energy of a system equals a variation of work and a variation of heat, Q_h [J], the overall energy being conserved. Note that the potential of a system to perform work is equivalent to *free energy*, while a variation in heat corresponds to the product of a variation in entropy S [J K^{-1}] and absolute temperature T [K], i.e., $\delta Q_h = T\,\delta S$, as introduced by Clausius (1857). The second law of thermodynamics states that entropy is produced during irreversible processes, while it cannot be consumed. This implies that isolated systems, which neither exchange mass, nor energy, nor entropy with their environment, reach a dead state of maximum entropy called thermodynamic equilibrium in which all potential gradients have been depleted. Kleidon (2016) distinguishes three types of physical entropy, i.e., thermal entropy produced by friction and depletion of temperature gradients, molar entropy produced by mixing and depletion of chemical potential/concentration gradients, and radiation entropy produced by radiative cooling and depletion of radiation temperature differences. From the first and second law of thermodynamics one can conclude that free energy is not conserved, as it corresponds to the variation in internal energy minus the variation in heat within a given time frame during which entropy is produced. Free energy dissipation and entropy production are thus inseparable, and maximization of the entropy of an isolated system occurs due to conservation of energy at the expense of minimizing its free energy. An open system may nevertheless persist in steady states of lower entropy if it is exposed to a sufficient influx of free energy to sustain the necessary physical work that needs to be performed to act against the natural depletion of the internal potential gradients, or even to steepen them and further reduce the entropy. Order in an open

system thus manifests through persistent gradients and an entropy lower than the maximum. Steps to higher order and lower entropies imply a steepening of internal gradients. This is exactly what occurs when preferential flow in groundwater emerges, as the fluid tends to concentrate in localized preferential pathways.

The free energy balance associated with groundwater fluxes can be formulated considering the free energy fluxes per unit area, $\boldsymbol{J}^E_{free}$ [J s^{-1} m^{-2}], and the amount of dissipated energy per volume, d [J s^{-1} m^{-3}], in the form:

$$\frac{\partial e_{free}}{\partial t} = -\nabla\cdot\boldsymbol{J}^E_{free} - d, \tag{1}$$

e_{free}[J m^{-3}] being free energy per unit volume. Advective fluxes of free energy forms associated with fluid flow in an aquifer are formed by three components: mechanical, $\boldsymbol{J}^E_H$, potential, $\boldsymbol{J}^E_{pot}$, and kinetic, $\boldsymbol{J}^E_{kin}$, energy fluxes, evaluated as:

$$\boldsymbol{J}^E_H = \mathbf{q}\rho g H; \quad \boldsymbol{J}^E_{pot} = \mathbf{q}\rho g z; \quad \boldsymbol{J}^E_{kin} = \mathbf{q}\rho\frac{v^2}{2}, \tag{2}$$

where $\mathbf{q}$ [m s^{-1}] is the groundwater flux vector, ρ[kg m^{-3}] is density of water; g [m s^{-2}] is gravitational acceleration; v [m s^{-1}] is the magnitude of fluid velocity; and H and z [m] are pressure head and geodetic elevation, respectively. Note that while kinetic energy is proportional to v^2, the kinetic energy flux corresponds to the product of the volumetric water flux $\mathbf{q}$ and its kinetic energy density, $\rho\, v^2/2$. Thus, the kinetic energy flux is proportional to v^3 and is very small in common groundwater flow conditions characterized by low values of the Reynolds' number. By inserting Eq. (2) into Eq. (1) and assuming a constant fluid density, we obtain:

$$\frac{\partial e_{free}}{\partial t} = -\rho g\ \nabla\cdot[\boldsymbol{q}(H+z)] - \frac{1}{2}\rho\nabla\cdot[\boldsymbol{q}v^2] - d. \tag{3}$$

Here, we consider a free surface aquifer, where flow is a gravity-driven process taking place over an impervious topographic surface, mechanical energy being neglected with respect to the other terms. In contrast to a setting associated with a river network, kinetic energy in a groundwater flow network can also be neglected (e.g., Loritz et al., 2019). Hence, considering Eq. (3), the energy dissipated per unit volume (i.e., per unit cross-section and per unit length of the preferential flow path) at steady-state conditions can be evaluated as:

$$d = -\rho g\ \mathbf{q}\cdot\nabla z. \tag{4}$$

Energy dissipation within a segment of length l_i along the network is given by:

$$D_i = \rho g Q_i |\nabla z_i|\, l_i, \tag{5}$$

where Q_i and $|\nabla z_i|$ are the groundwater discharge and the local slope associated with segment l_i, respectively. The total dissipation of free energy within the network upstream of a given point (or section) corresponds to the sum of D_i over all segments conveying to such a point (or section).

The trivial solution that minimizes dissipation is the case of a zero discharge in the network. A non-trivial solution requires an assumption about the way the Q_i is growing along the network. Considering a spatially uniform and steady-state recharge, r, leads to $Q_i = rA_i$, A_i being the upstream catchment area (see also Rodriguez-Iturbe et al., 1992 for additional details), expressed hereafter as pixels accumulation $A_i = A(\mathbf{x}_i)$ [-] (in cell units), i.e., as the sum of upstream pixels k conveying flow to pixel i (Balister et al., 2018):

$$A_i = A(\mathbf{x}_i) = \sum_{k=1}^{Np-1} W_{ki}\, A(\mathbf{x}_k) + 1, \tag{6}$$

where $(N_p - 1)$ is the number of pixels conveying groundwater flow to pixel i, and W_{ki} is the *connectivity matrix* for a given realization of the topographic surface. Non-zero entries of W_{ki} correspond to all subsets of connected pixels evaluated for each topography realization. Note that quantity $A_i = A(\mathbf{x}_i)$ corresponds to the number of pixels connected to a given reference pixel i in the domain.

We recall that the theory of optimal channel networks (OCNs) is based on an empirical power-law formulation relating A_i and the local slope of the topographic surface, i.e.:

$$A_i^{\gamma}|\nabla z_i| = const \rightarrow |\nabla z_i| \propto Q_i^{-\gamma}. \tag{7}$$

where the value of γ is comprised in the unit interval. Studies based on the analysis of river networks (e.g., Hack, 1957; Tarboton et al., 1989; Banavar et al., 2000) suggest a value of γ approximately equal to 0.5. With reference to a groundwater system, Hergarten et al. (2014) assume a power law relationship between conductivity (K) and porosity (ϕ), i.e., $K \propto \phi^n$, and show that an optimal distribution of porosities and conductivities (Eqs. (29)-(30) of Hergarten et al., 2014) can be obtained when $\gamma = (n-1)/(n+1)$. The value of the exponent n ($\geq$2) is site-specific. As an example, Riva et al. (2008), on the basis of K and ϕ laboratory data obtained from drilled core samples collected within an alluvial system in the Neckar river valley (Germany), estimate n = 2.857, thus leading to γ = 0.481. Thus, while the topic deserves additional detailed studies and we do not pursue it further in this study, considering $\gamma \approx 0.5$ appears as a plausible interpretive choice also for PGNs.

Substituting Eq. (7) into Eq. (5), yields

$$D_i \propto \rho g |\nabla z_i|^{1-1/\gamma}\, l_i. \tag{8}$$

Therefore, according to Eq. (8), a PGN (in a way similar to what has been shown for the identification of OCNs in the context of river networks, see, e.g., Balister et al., 2018) can be constructed by driving subsurface flow along directions associated with the steepest gradients of the aquifer bottom topography.

In Section 3 we rely on each topography realization of the aquifer bottom (see Section 2.2) to delineate a collection of networks described as connected subsets of pixels to form an oriented tree-like topology. A given pixel i of a network associated with a topography realization, i.e., $\mathbf{x}_i(x_i, y_i)$, is surrounded by up to eight j neighboring pixels through a corresponding number of links, each denoted as ℓ_i, and forming a S_i neighborhood of j links. The Euclidean distance l_i associated with the link ℓ_i between adjacent pixels $\mathbf{x}_j$ and $\mathbf{x}_i$ is taken as $l_i = aL$, where L is the characteristic pixel size, a being equal to 1 or $\sqrt{2}$ when moving along directions parallel to the sides or to the diagonal of a given square pixel, respectively. Delineation of the PGN for each realization of the aquifer bottom requires treating isolated pixels (typically termed *pits* or no-escape flow cells) on the topographic surface through the application of a correction term, the latter being embedded in a *Pit Removal algorithm* (Tarboton et al., 1989; Tarboton, 2013). The direction of groundwater flow from a cell j to an adjacent cell i is then evaluated upon ensuring the largest elevation drop, i.e.:

$$\Delta z(\mathbf{x}_{j,i}) = \max_{i,j\ \in\ S_i}\{z(\mathbf{x}_j) - z(\mathbf{x}_i)\}. \tag{9}$$

Consistent with the analyses of Rodriguez-Iturbe et al. (1992), Rodriguez-Iturbe and Rinaldo (2001) and Balister et al. (2018) in the context of surface flow in OCNs, we term PGN the collection of j pixels connected with a given pixel i and satisfying Eq. (9). While Eq. (9) does not necessarily minimize dissipation, it is a necessary condition to maximize power in the groundwater flow setting considered. It can then be noted that, even when the Optimal Channel Network (OCN) observed at the current time is indeed a network that minimizes dissipation (and thus power in groundwater flow along the network is maximized), it is also the fingerprint of the work the fluid has performed in the past (during generally unsteady flow conditions). Hence, in line with Kleidon et al. (2013) or Zehe et al. (2021), we would argue that PGNs have developed along pathways that locally maximize power in groundwater flow.

Amongst existing cell-based grid models developed to determined

drainage networks (e.g., Tarboton et al., 1997; Orlandini et al., 2003), here we apply the commonly used D8 method (O'Callaghan and Mark, 1984). Identification of a PGN for a given topography realization requires introducing an area-based threshold (see, e.g., Dietrich et al., 1992; Dietrich et al., 1993). From an operational standpoint, this corresponds to setting the minimum number of connected pixels conveying fluid to a target one, according to the criterion embedded in Eq. (9). The collection of pixels for which the imposed threshold value is exceeded are then elected as part of the PGN in the considered Monte Carlo realization of the topography. We delineate a PGN for each topography realization across the considered Monte Carlo collection and evaluate the probability $\chi(\mathbf{x}_i)$ that pixel $\mathbf{x}_i$ is located on a connected path. This enables us to obtain a stochastic description of the spatial distribution of preferential groundwater flow pathways that embeds minimization of energy principles and is constrained by the amount of available information about the topography of the bottom of a target aquifer.

3. Results

3.1. Stochastic simulations of Preferential Groundwater Networks (PGNs)

Stochastic (conditional) realizations of the topography of the free surface aquifer bottom are based on the dataset described in Section 2.1. The elevation of the aquifer bottom is modeled as a spatial random field, characterized in terms of a given structure of the associated variogram. The latter is assessed through the available elevation data and is described through an isotropic gaussian model:

$$\Gamma(h) = \sigma_n^2 \exp\left(1 - 3h^2/a^2\right), \tag{10}$$

where $h = \|\mathbf{x} - \mathbf{x}'\|$ is separation distance between vector locations $\mathbf{x}$ and $\mathbf{x}'$; σ_n^2 and a are model parameters, corresponding to the variogram sill and range, respectively. Here, we estimate the former as the variance of the available data, the ML estimate of the latter being $a = 7.80$ km (lower and upper bounds of the associated 95% ML-based confidence interval being 7.35 and 8.25 km, respectively).

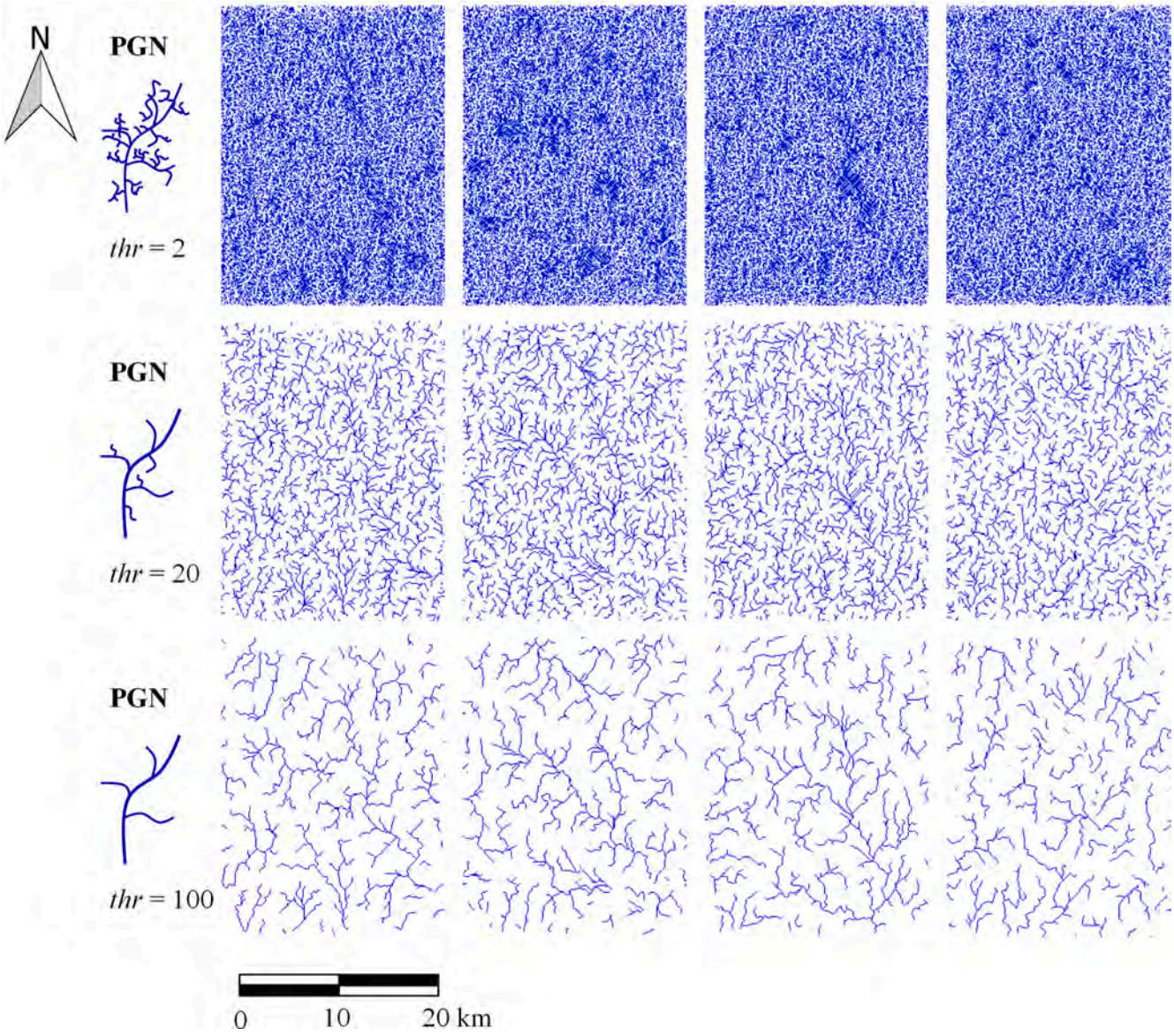

Fig. 2. Exemplary PGNs for the whole study area obtained from four selected topography realizations and corresponding to 3 diverse area-based threshold values, i.e., *thr* = 2, 20, and 100 pixels.

We (*a*) generate a collection of *NMC* = 2000 MC realizations of aquifer bottom topography through the approach described in Section 2.2 and (*b*) apply Eq. (9) and the methodology described in Section 2.3 to construct a PGN for each topography realization. In our exemplary application, we consider the effect of three diverse values of area-based thresholds, corresponding to *thr* = 2, 20, and 100 pixels, respectively, and obtain three MC-based collections of PGNs for the area of study. Fig. 2 depicts four exemplary PGNs extracted from the corresponding topography realizations upon considering the selected area-based threshold values. The morphology of the network is affected by the selected threshold value, higher values of the latter enabling one to clearly delineate the main connected branches of the subsurface pathways, consistent with the definition of threshold.

We recall that an increased level of detail in the description of a network, corresponding to lowest threshold values, yields a high probability that a randomly selected pixel in the domain belongs to a PGN. Otherwise, coarser networks (such as those resulting from a high threshold and corresponding to identifying the major pathways across the domain) lead to a lower probability that a randomly selected pixel belongs to a PGN. As an example of the type of results that can be obtained, Fig. 3 juxtaposes the PGN associated with *thr* = 100 pixels and resulting from the average topography obtained across the MC topography realizations, hereafter termed PGN_{thr}, and a color map depiction of the spatial distribution of the probability, $\chi(\mathbf{x}_i)$, that a given pixel $\mathbf{x}_i$ belongs to the PGN associated with the same threshold value. Fig. 4 includes corresponding depictions obtained upon setting *thr* = 2 or 20 pixels. High values of $\chi(\mathbf{x}_i)$ correspond to a high probability that a pixel be carved by a PGN. We note that relying on *NMC* = 2000 MC realizations yield stable results for all of the threshold values considered (details not shown).

Similar to standard practice in surface hydrology, a PGN closure section can be defined as a pixel or a segment comprising several pixels where a PGN conveys subsurface flow according to the steepest gradients of bottom topography, as discussed in Section 2.3. We recall that

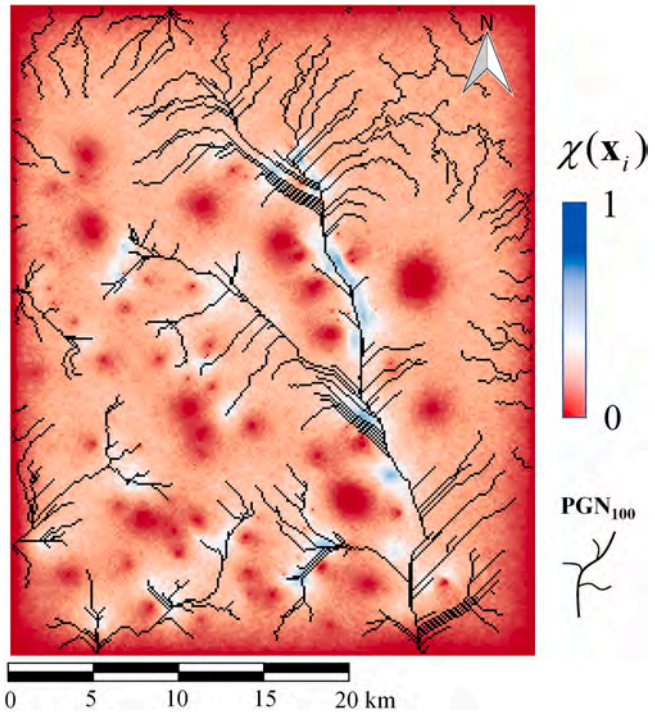

Fig. 3. PGN resulting from threshold *thr* = 100 pixel evaluated for the whole study area and considering the average topography computed across the MC realizations (PGN_{100}, black curves), juxtaposed to the spatial distribution of the probability, $\chi(\mathbf{x}_i)$, that a given pixel $\mathbf{x}_i$ belongs to the PGN.

higher threshold values favor the sharp delineation of the main branches of a PGN in a given realization as opposed to what could be observed in the presence of a low threshold value. Furthermore, pixels which are connected along a PGN delineated with a higher threshold are characterized by values of bottom elevation that are closer to the global energy minimum of the PGN, i.e., the bottom elevation of the closure section. Thus, higher values of the imposed threshold lead to fewer pixels which are likely to belong to a PGN and are all characterized by elevations which are closer to the one of the network outlet. This behavior is reflected by the probability maps depicted in Figs. 3 and 4, where one can note that values of $\chi(\mathbf{x}_i)$ tend to span across an increased range with decreasing threshold. Additionally, one can note that the juxtaposed PGN_{100} evidences that the main branches of the network across which subsurface flow is conveyed are associated with pixels where probability values across MC realizations, i.e., $\chi(\mathbf{x}_i)$, are the highest.

Fig. 5 juxtaposes PGN_{100} to the available piezometric contour map. The reconstruction of the piezometric surface is mainly available in the southern region (i.e., the most productive area in the region, see also Section 2.1), which is mainly composed by sand and gravel alluvial geomaterials. Fig. 5 enables us to assess the correspondence between the subsurface flow pattern resulting from an analysis grounded on the energy-based approach we consider and what can be inferred from the analysis of typically available piezometric data. Results encapsulated in Fig. 5 suggest the subsurface network carved from energy-based concepts closely corresponds to the main flow directions (represented as blue arrows) associated with the available piezometric reconstruction. On the basis of Fig. 3, a similar conclusion can be drawn upon considering the MC-based probabilistic results quantifying the spatial distribution of the probability associated with preferential pathways across the domain. Examples of local scenarios are offered in the insets of Fig. 5, where one can clearly see that the approach can (*i*) capture the main subsurface flow patterns (insets A and C green arrows) as inferred by available piezometric data (insets A and C, blue arrows) and (*ii*) offer an assessment of subsurface flow directions when piezometric data are not available (insets B and C, green arrows). In the latter case, Fig. 5 suggests the presence of subsurface recharge from the aquifer to surface water bodies (the lakes and the Adda river) close to the city of Lecco (inset B), as well as the emergence of a subsurface connection between two lakes (*Pusiano* and *Annone* lakes; inset C).

Our probabilistic results enabling the delineation of the main subsurface flow networks under uncertainty are also consistent with the available geological information. We analyze these aspects upon comparing the spatial location of PGNs obtained on the basis of the average MC-based topography of the aquifer bottom and the three threshold values analyzed (i.e., PGN_2, PGN_{20}, PGN_{100}) against the geological scenarios emerging from the reconstructed geological cross-sections (located as in Fig. 1). As an example, Fig. 6 juxtaposes the geological *Section Y.Y* (see Fig. 1) and the spatial location of PGN_2, PGN_{20}, PGN_{100}. For completeness, the probability $\chi(\mathbf{x}_i)$ evaluated upon the complete collection of MC-based topography realizations is also included.

These results suggest that the identified PGNs are generally comprised within alluvial sedimentary subsurface basins where hydrofacies are mainly composed by highly permeable geomaterials, as highlighted here by dashed boxes. We further note that the highest values of $\chi(\mathbf{x}_i)$ correspond, in general, to areas where the aquifer is mainly composed by alluvial and fluvioglacial geomaterials, which are typically highly conductive. Results of similar quality are obtained for all of the remaining cross-sections (not shown), thus imbuing us with confidence about the reliability of our approach and its consistency with available geological information.

Fig. 7a depicts empirical probability density functions (pdfs) of χ evaluated across the whole domain for *thr* = 2, 10, 20, 50, and 100 pixels. The pdf of χ exhibits two peaks: (*i*) a first peak is located at $\chi = 0$, corresponding to pixels which are not located on a connected path in any of the realizations; and (*ii*) a second peak corresponds to values of χ that

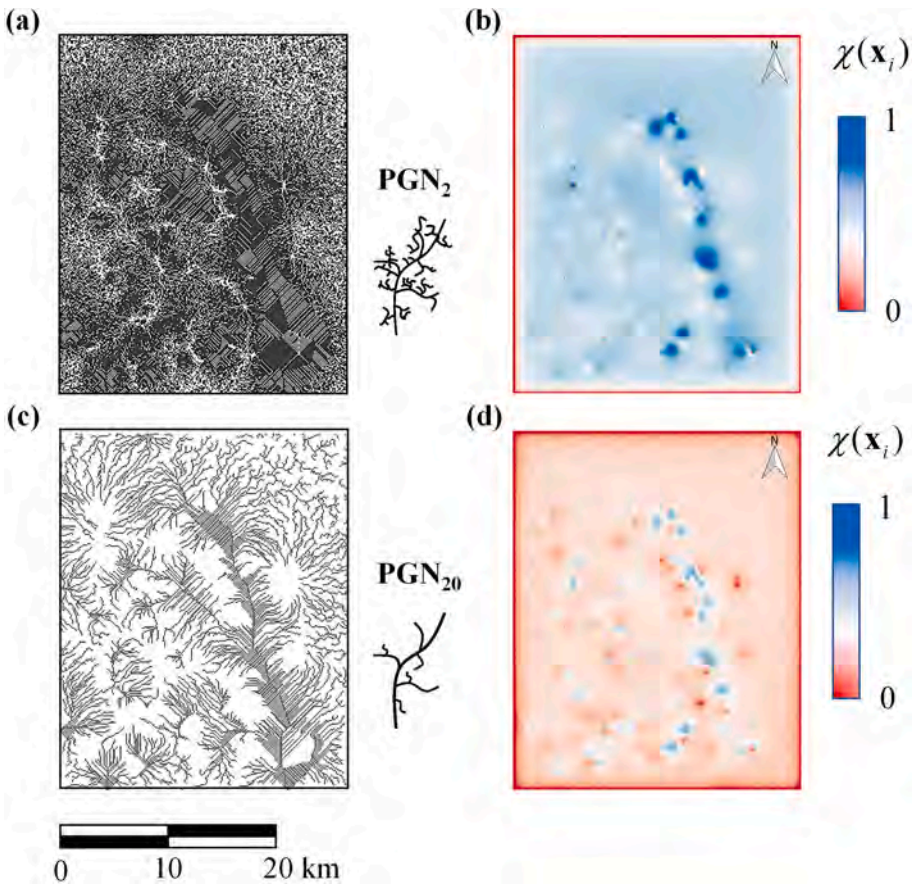

Fig. 4. PGNs resulting from threshold *thr* = (*a*) 2 (PGN_2) and (*c*) 20 (PGN_{20}) pixels evaluated for the whole study area and considering the average topography computed cross the MC realizations. Spatial distribution of the probability, $\chi(\mathbf{x}_i)$, that a given pixel $\mathbf{x}_i$ belongs to the PGN for *thr* = (*b*) 2 and (*d*) 20 pixels.

decrease with increasing threshold (i.e., the most frequent value of χ decreases as *thr* increases, shifting from about 50% to 5% for *thr* = 2 or 100, respectively). The probability that $\chi > 0$ is almost constant with *thr* and is equal to about 97%. In other words, only 3% of the domain is characterized by pixels that do not belong to a connected path in at least one realization. Fig. 7b depicts the empirical pdf of χ conditional to the observation that a given pixel of the ensemble belongs to a connected path in at least in one realization (i.e., $\chi > 0$) in terms of the rescaled variable $(\chi - \mu_\chi)/\sigma_\chi$, μ_χ and σ_χ being mean and standard deviation of $\chi > 0$, respectively. The dependence of first four statistical moments of the pdf of χ and of $\chi > 0$ on *thr* is depicted in Fig. 8a (μ_χ, σ_χ, and kurtosis, κ_χ) and 8b (skewness, s_χ). One can observed that the conditional statistical moments are not dramatically different from their unconditional counterparts. In particular, the unconditional and conditional means almost coincide. Values of μ_χ, σ_χ, and κ_χ tend to decrease as the threshold value increases according to a power law expression, i.e., they are proportional to thr^{-b} (estimated values of *b* are also listed in Fig. 8a). These findings are qualitatively consistent with the previously documented decrease of the probability that a pixel is carved by a PGN for increased threshold values, as well as with the observation that the delineated subsurface network is spatially coarser (as only the major branches are delineated) for increasing threshold (see also Figs. 3 and 4). PGNs delineated upon considering a low threshold value are typically associated with a wider range of values of χ than those stemming from higher thresholds, this being consistent with the increased values of σ_χ and κ_χ (the latter reflecting the occurrence of heavier tails) related to low thresholds. On the other hand, the skewness of χ increases with *thr*, i.e., sample distributions of χ are seen to transition from negatively (left tailed) to positively (right tailed) skewed with increasing threshold, attaining a zero skewness (symmetric distribution) for *thr* ≈ 50 pixels in our case. In general, we note that all moments appear to stabilize at *thr* ≈ 40, with an exception for skewness that does not reach a near-constant value as *thr* increases.

Finally, we recall (see Section 3.1) that pixels on a PGN stemming from a large threshold value are associated with elevation values which are lowest and closest to the global minimum elevation in the system. Due to the nature of the network, pixels close to a closure section are typically characterized by a lower bottom gradient value than those far from it, as supported by Eq. (7). These elements can be grasped, for example, when analyzing PGN_2 and PGN_{100} (Figs. 3 and 4) and noting that pixels belonging to the former network are characterized by low values of the accumulation function (Eq. (6)) and are related to elevations which can be markedly diverse from the one of the closure section. As stated above, one can then see that the average value of χ decreases with increasing *thr* because of its dependence on the local values of the accumulation function and, in turn, on pixel elevations (see Section 2). Thus, pixels characterized by lower elevation and higher value of the accumulation function tend to be related to an increased probability of residing on a PGN. This behavior is related to the slope-driven nature considered for the subsurface flow, which is fully consistent with energy minimization concepts (Rodriguez-Iturbe and Rinaldo, 2001) of the kind that are observed in river network studies. We further note that the estimated value of *b* (=0.566) associated with μ_χ is slightly larger than the typical values observed in dendritic networks (i.e., ≈ 0.43–0.5; Hergarten et al., 2016). This behavior can be due to (*i*) the finite size of the sample and/or (*ii*) a certain degree of spatial correlation embedded in the elevation of the aquifer bottom, the latter being correlated in space, and/or (*iii*) a combination of these two effects.

The analysis of the way statistical moments of χ vary with *thr* can then complement the appraisal of the degree of spatial coverage of the

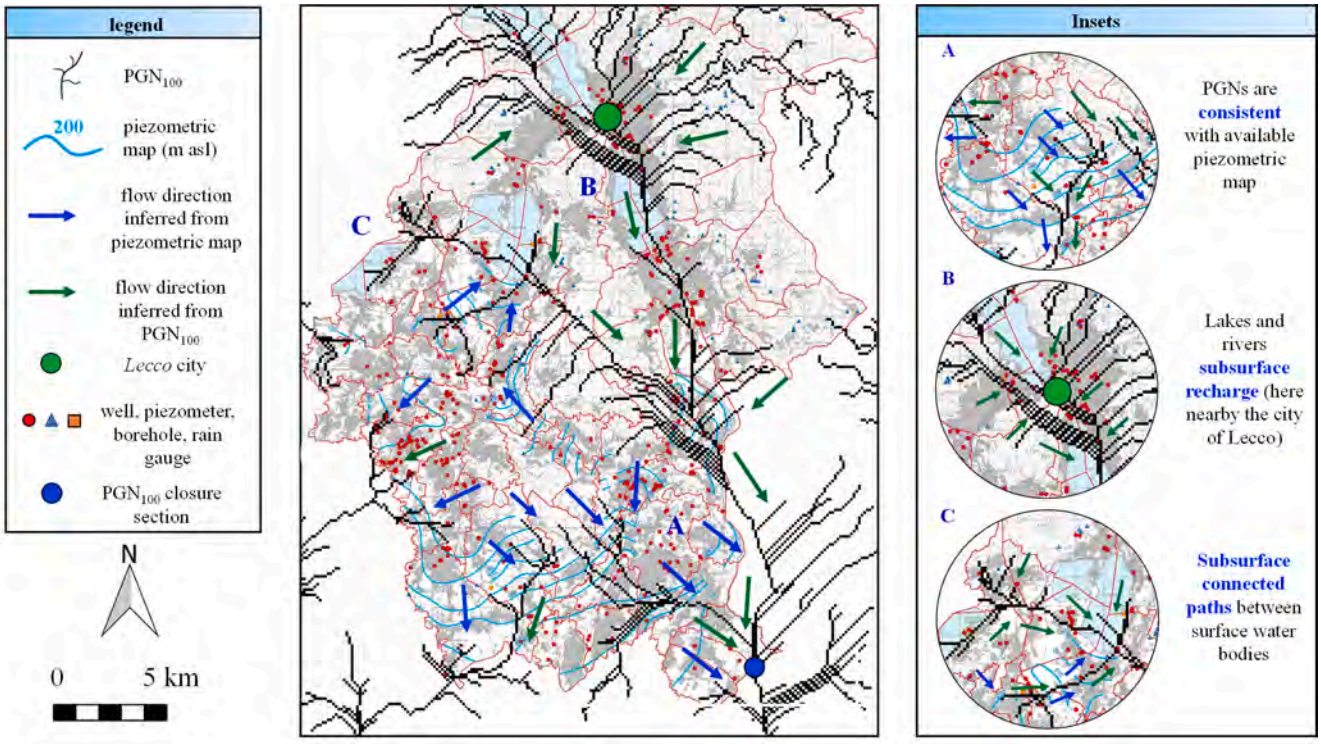

Fig. 5. PGN_{100} and available piezometric contour map (light blue curves). Insets correspond to enlargements of local scenarios. Arrows correspond to the main subsurface flow directions inferred from the piezometric map (in blue) and from the PGNs (in green). (For interpretation of the references to color in this figure legend, the reader is referred to the web version of this article.)

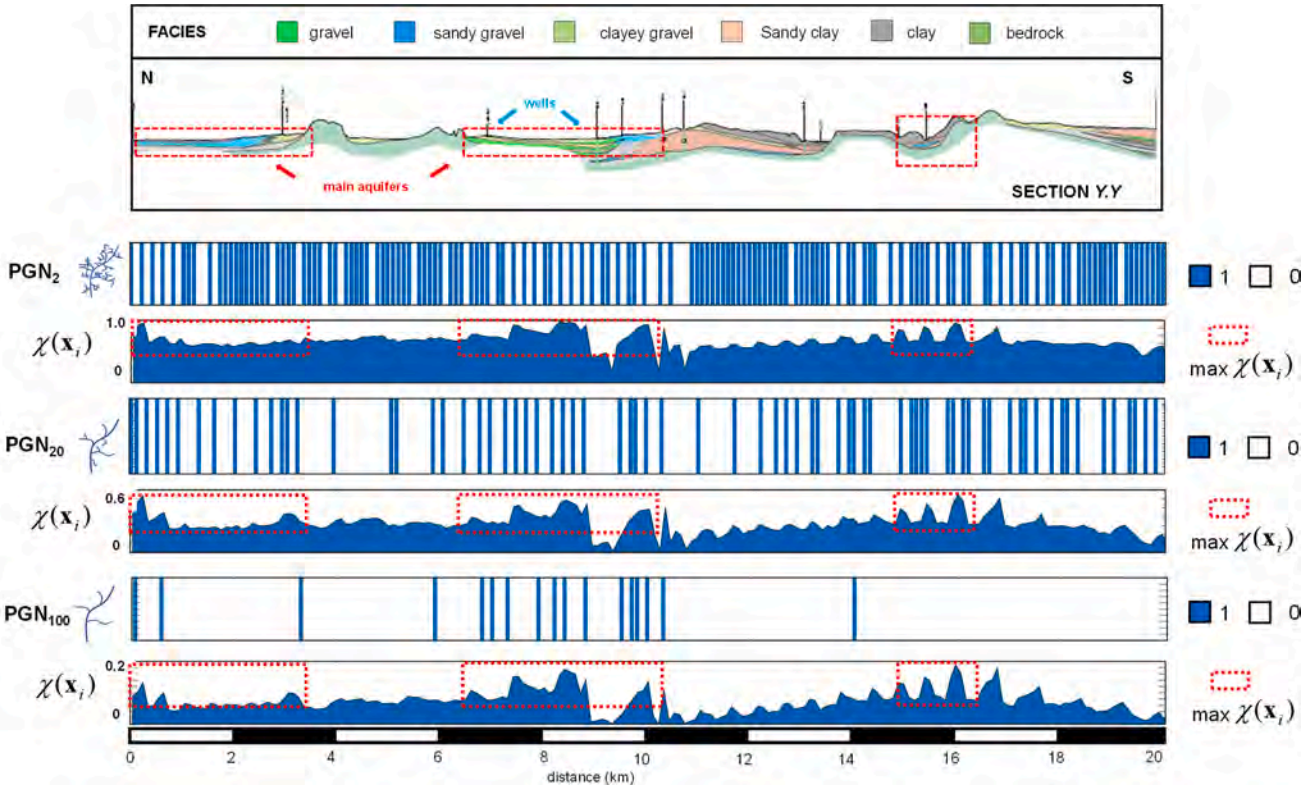

Fig. 6. Hydrogeological *Section Y.Y* (see Fig. 1) and spatial location of PGN_2, PGN_{20}, and PGN_{100}. Values of probability $\chi(\mathbf{x}_i)$ evaluated across the complete collection of MC-based topography realizations is also included, the largest values of $\chi(\mathbf{x}_i)$ being highlighted by red dashed boxes. Note that each subplot depicting $\chi(\mathbf{x}_i)$ is characterized by a different scale, for clarity of illustration. (For interpretation of the references to color in this figure legend, the reader is referred to the web version of this article.)

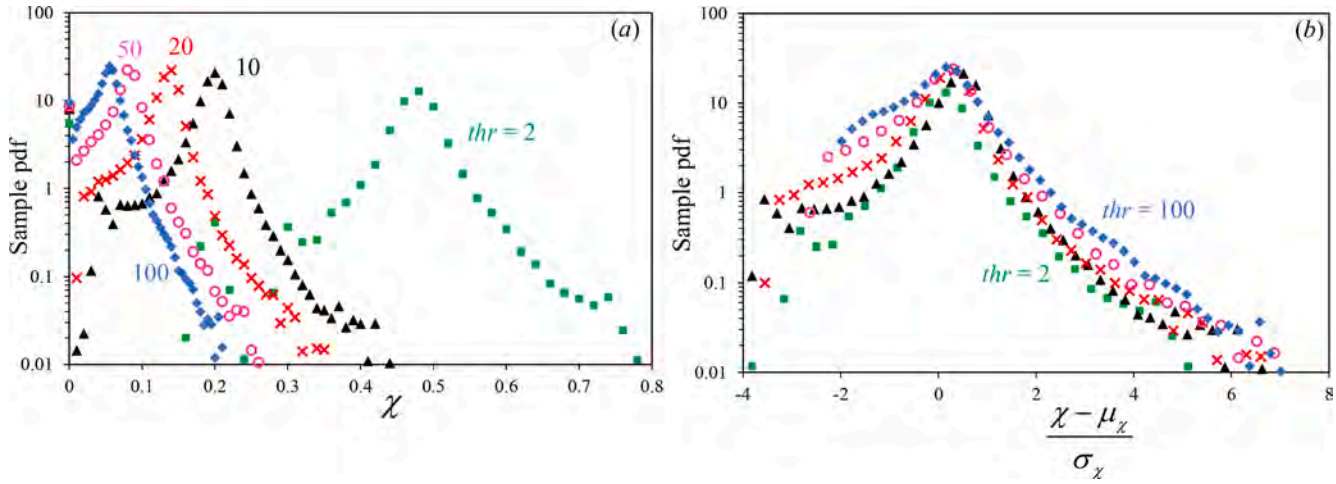

Fig. 7. Sample pdf of (*a*) χ and (*b*) $\chi > 0$ across the whole domain for *thr* = 2, 10, 20, 50, and 100 pixels.

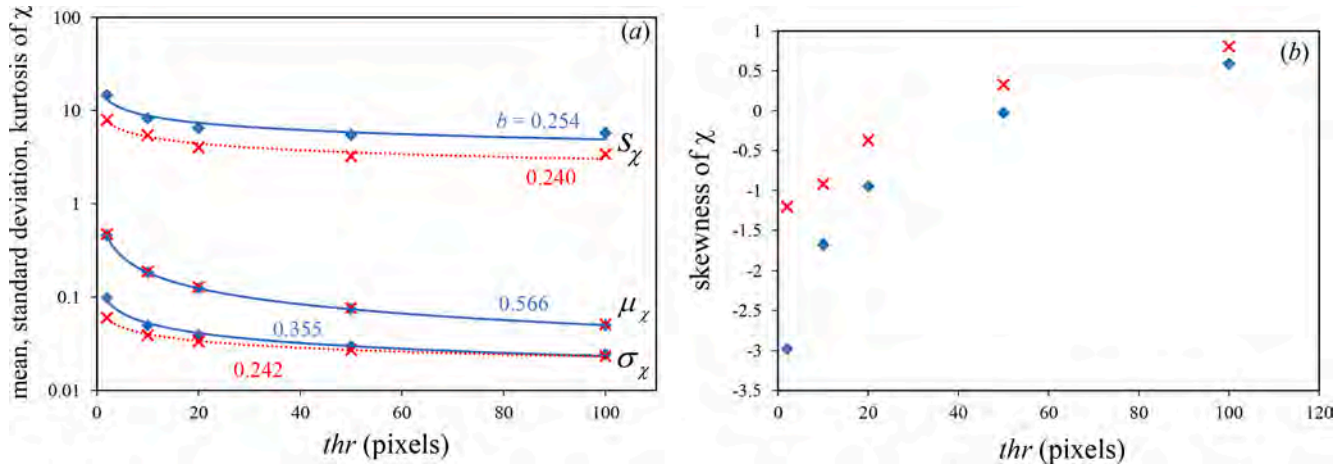

Fig. 8. First four statistical moments of χ (blue symbols) and of $\chi > 0$ (red symbols) versus *thr*. The power law trend thr^{-b} (blue curves for χ and red curves for $\chi > 0$) is depicted in (a) together with estimated values for *b*. (For interpretation of the references to color in this figure legend, the reader is referred to the web version of this article.)

preferential network. The decrease of the variance of χ with *thr* clearly documented in Fig. 8a is consistent with the observation that a PGN carved by a large value of *thr* connects a reduced number of pixels which are in turn associated with elevations which are closer to the one of the closure, as opposed to what can be expected upon considering a low *thr*. As such, PGNs resulting from low thresholds are also seen to comprise pixels within a broad range of bottom elevations, thus giving rise to an increased energy consumption along the network. At the same time, the low values of kurtosis of χ documented for the largest threshold considered (i.e., *thr* = 50 and 100) are also consistent with the energy-related nature of an extracted PGN. Large values of *thr* tend to exclude branches conveying low flow rates through the network and tend to include solely the main branches of the network, this, in turn, being reflected onto a decrease of the tails of the pdf of χ.

4. Discussion and conclusions

In this study we characterize key features of subsurface flow paths from an energetic and probabilistic perspective. We provide evidence that subsurface flow in a free aquifer system is mainly governed by spatial gradients of the aquifer bottom topography, the latter being inferred through (Monte Carlo based) stochastic simulations relying on stratigraphic observations. Our approach enables one to identify *Preferential Groundwater Networks* (PGNs), which correspond to the major pathways along which subsurface flow is conveyed. PGNs are extracted by locally (*a*) following the steepest gradient associated with the aquifer bottom topography related to random realizations conditional on the available information and (*b*) considering the influence of diverse values of area threshold employed for their delineation. We find that PGNs inferred from the averaged bottom topography with the highest area threshold considered are strikingly consistent with main flow directions inferred from available piezometric data and key subsurface flow patterns (such as subsurface connectivity between surface water bodies) resembling the overall behavior that can be inferred from visual inspection of the system. Location of PGNs is furthermore consistent with geological and hydrogeological information at our disposal, such as geological data (and ensuing hydrogeological sections) and is coherent with the nature of the aquifers investigated.

The idea that that preferential flow implies a reduced dissipation in fluid flow and that the fluid moves along an optimized river network (Howard, 1990) or rill network topologies (Rieke-Zapp and Nearing, 2005) has been broadly discussed in the context of surface hydrology scenarios. Preferential flow leads to faster fluid flows because they reduce dissipative losses due to an increased hydraulic radius in the rill or river network as compared to sheet flow (Berkowitz and Zehe, 2020). Subsurface preferential flow of water reduces dissipative losses as well (Zehe et al., 2010; Zehe et al., 2013), as friction occurs mainly at macropore or fracture walls, while frictional interactions in the matrix take

place along the entire inner surface across the system. Reduced dissipation and faster fluid flow imply a more energy efficient throughput of water, mass, and chemical species through the entire system (in case of flow paths spanning the entire system).

The positive feedback that might lead to a growth of PGN minimizing total energy dissipation is not obvious. In this context, it is then striking that the PGNs identified in this study display a qualitatively good consistency with macroscale flow paths and characteristics of the free aquifer systems inferred from standard piezometric maps available in the area.

We thus conclude that the approach we consider to infer PGNs in subsurface flow interpretation is methodologically sound as well as operationally robust. Our study illustrates the breadth and the potential of the approach, which is seen as a potentially powerful and flexible tool to assist interpretation of the main traits of large-scale subsurface flows. These findings will serve as basis for further research, oriented towards enhanced understanding of subsurface hydrology through the framework of energy-optimal networks.

5. Data source

All source data, cartographic information and piezometric map we used can be found from *Regione Lombardia Geoportale* within *Data Download* Section (https://www.geoportale.regione.lombardia.it/download-dati).

6. Software packages

Subsurface topography realizations have been performed through SGEMS software (GSLIB library), freely available at https://sgems.sourceforge.net/?q = node/77.

Topography-based networks have been obtained through the software TauDEM, freely available at https://hydrology.usu.edu/taudem/taudem5/downloads.html.

All computations and Figures have been realized in MATLAB R2019a environment (https://www.mathworks.com/products/new_products/release2019a.html) through an institutional license, while data spatial representation has been organized within QGIS 2.18 environment (https://qgis.org/en/site/forusers/download.html).

CRediT authorship contribution statement

Massimiliano Schiavo: Conceptualization, Data curation, Formal analysis, Investigation, Methodology, Validation, Visualization, Writing – original draft, Writing – review & editing. **Monica Riva:** Conceptualization, Data curation, Formal analysis, Investigation, Methodology, Validation, Visualization, Writing – original draft, Writing – review & editing. **Laura Guadagnini:** Conceptualization, Data curation, Formal analysis, Investigation, Methodology, Validation, Visualization, Writing – original draft, Writing – review & editing. **Erwin Zehe:** Conceptualization, Data curation, Formal analysis, Investigation, Methodology, Validation, Visualization, Writing – original draft, Writing – review & editing. **Alberto Guadagnini:** Conceptualization, Data curation, Formal analysis, Investigation, Methodology, Validation, Visualization, Writing – original draft, Writing – review & editing.

Declaration of Competing Interest

The authors declare that they have no known competing financial interests or personal relationships that could have appeared to influence the work reported in this paper.

Acknowledgments

Lario Reti Holding is gratefully acknowledged for providing key funding to the development of the research.

The authors are grateful to Dr. Stefan Hergarten and to an anonymous Reviewer whose suggestions helped improving and clarifying the study.

References

Balister, P., Balogh, J., Bertuzzo, E., Bollobás, B., Caldarelli, G., Maritan, A., Mastrandrea, R., Morris, R., Rinaldo, A., 2018. River landscapes and optimal channel networks. PNAS 115 (26), 6548–6553. https://doi.org/10.1073/pnas.1804484115.

Banavar, J.R., Colaiori, F., Flammini, A., Maritan, A., Rinaldo, A., 2000. Topology of the Fittest transportation Network. Phys. Rev. Lett. 84 (20), 4745–4748.

Beretta, G.P., Denti, E., Francani, V., Sala, P., 1984. Lineamenti idrogeologici del settore sublacquale della provincia di Como. Acque Sotterranee 1 (4), 23–62.

Berkowitz, B., Zehe, E., 2020. Surface water and groundwater: unifying conceptualization and quantification of the two "water worlds". Hydrol. Earth Syst. Sci. 24, 1831–1858. https://doi.org/10.5194/hess-24-1831-2020.

Bianchi Janetti, E., Guadagnini, L., Riva, M., Guadagnini, A., 2019. Global sensitivity analyses of multiple conceptual models with uncertain parameters driving groundwater flow in a regional-scale sedimentary aquifer. J. Hydrol. 574, 544–556.

Camporese, M., Paniconi, C., Putti, M., McDonnell, J.J., 2019. Fill and spill hillslope runoff representation with a Richards equation-based model. Water Resour. Res. 55 (11), 8445–8462.

Cavallin A., Francani V., Mazzarella S., 1983. Studio idrogeologico della pianura compresa tra Adda e Ticino, CAP Milano.

Clausius, R., 1857. Über die Art der Bewegung, die wir Wärme nennen, Annalen der Physik, 100 (3): 353–379, Bibcode:1857AnP176353C, doi:10.1002/andp.18571760302.

D'Odorico, P., Rigon, R., 2003. Hillslope and channel contributions to the hydrologic response. Water Resour. Res. 39 (5), 1113. https://doi.org/10.1029/2002WR001708.

Deutsch, C.V., Journel, A.G., 1997. GSLIB: Geostatistical Software Library and User's Guide. Oxford University Press, New York. https://doi.org/10.4236/oalib.1106672.

Dietrich, W.E., Wilson, C.J., Montgomery, D.R., McKean, J., Bauer, R., 1992. Erosion thresholds and land surface morphology. Geology 20 (8), 675.

Dietrich, W.E., Wilson, C.J., Montgomery, D.R., McKean, J., 1993. Analysis of Erosion Thresholds, Channel Networks, and Landscape Morphology Using a Digital Terrain Model. The Journal of Geology 101 (2), 259–278.

Hack, J. T., 1957. Studies of longitudinal profiles in Virginia and Maryland. US Geol. Survey Prof. Papers, 294-B, U.S. Government Printing Office, Washington, D.C.

Hergarten, S., Winklerm, G., Birk, S., 2014a. Transferring the concept of minimum energy dissipation from river networks to subsurface flow patterns. Hydrol. Earth Syst. Sci. 18, 4277–4288. https://doi.org/10.5194/hess-18-4277-2014.

Hergarten, S., Winklerm, G., Birk, S., 2014b. Scale invariance of subsurface flow patterns and its limitation. Water Resour. Res 52, 3881–3887. https://doi.org/10.1002/2015WR017530.

Howard, A.D., 1971. Optimal angles of stream junctions: geometric stability to capture and minimum power criteria. Water Resour. Res. 7, 863–873.

Howard, A.D., 1990. Theoretical Model of optimal Drainage Networks. Water Resour. Res. 26 (9), 2107–2117.

Kleidon, A., 2016. Thermodynamic foundations of the Earth system. New York NY: Cambridge University Press. doi: 10.1017/CBO9781139342742.

Kleidon, A., Zehe, E., Ehret, U., Scherer, U., 2013. Thermodynamics, maximum power, and the dynamics of preferential river flow structures at the continental scale. Hydrol. Earth Syst. Sci. 17, 225–251. https://doi.org/10.5194/hess-17-225-2013.

Leopold, Luna B., Langbein, Walter B., 1962. The concept of entropy in landscape evolution. US. geol. Surv. Prof. Paper (500-A).

Loritz, R., Kleidon, A., Jackisch, C., Westhoff, M., Ehret, U., Gupta, H., Zehe, E., 2019. A topographic index explaining hydrological similarity by accounting for the joint controls of runoff formation. Hydrol. Earth Syst. Sci. 23 (3807–3821), 2019. https://doi.org/10.5194/hess-23-3807-2019.

MacKie, E.J., Schroeder, D.M., Zuo, C., Yin, Z., Caers, J., 2020. Stochastic modeling of subglacial topography exposes uncertainty in water routing at Jakobshavn Glacier. Journal of Glaciology 67 (261), 75–83.

Orlandini, S., Moretti, G., Franchini, M., Aldighieri, B., Testa, B., 2003. Path-based methods for the determination of nondispersive drainage directions in grid-based digital elevation models. Water Resour. Res. 39 (6) https://doi.org/10.1029/2002WR001639.

O'Callaghan, J.F., Mark, D.M., 1984. The Extraction of Drainage Networks from Digital Elevation Data. Comput. Vis. Graph. Image Process. 28, 328–344. https://doi.org/10.1016/S0734-189X(84)80011-0.

Orlandini, S., Moretti, G., 2009. Determination of surface flow paths from gridded elevation data. Water Resour Res. 45 https://doi.org/10.1029/2008WR007099.

Reis, A.H., 2006. Constructal view of scaling laws of river basins. Geomorphology 78, 201–206. https://doi.org/10.1016/j.geomorph.2006.01.015.

Rieke-Zapp, D.H., Nearing, M.A., 2005. Slope shape effects on erosion: a laboratory study. Soil Sci. Soc. Am. J. 69, 1463–1471. https://doi.org/10.2136/sssaj2005.0015.

Rinaldo, A., Maritan, A., Colaiori, F., Flammini, A., Rigon, R., Rodriguez-Iturbe, I., Banavar, J.R., 1996. Thermodynamics of fractal networks. Phys. Rev. Lett. 76 (18), 3364–3367.

Rinaldo, A., Banavar, J.R., Maritan, A., 2006. Trees, networks and hydrology. Water Resour. Res. 42, 88–93. https://doi.org/10.1029/2005WR004108.

Riva, M., Guadagnini, A., Fernandez-Garcia, D., Sanchez-Vila, X., Ptak, T., 2008. Relative importance of geostatistical and transport models in describing heavily tailed

breakthrough curves at the Lauswiesen site. J. Contam. Hydrol 101, 1–13. https://doi.org/10.1016/j.jconhyd.2008.07.004.

Rodriguez-Iturbe, I., Rinaldo, A., Levy, O., 2001. Fractal River basins: chance and self-organization. Cambridge. doi 51 (7), 70–71.

Rodriguez-Iturbe, I., Rinaldo, A., Rigon, R., Bras, R.L., Marani, A., Vasquez, E.I., 1992. Energy Dissipation, Runoff Production, and the Three-Dimensional Structure of River Basins. Water Resour. Res. 28 (4), 1095–1103. https://doi.org/10.1029/91wr03034.

Schroers, S., Eiff, O., Kleidon, A., Scherer, U., Wienhöfer, J., Zehe, E., 2021. Morphological controls on Hortonian surface runoff: An interpretation of steady-state energy patterns, maximum power states and dissipation regimes within a thermodynamic framework. In: Hydrol. Earth Syst. Sci. Discuss. [under review for HESS]. https://doi.org/10.5194/hess-2021-479.

Tarboton, D.G., Bras, R.L., Rodriguez-Iturbe, I., 1989. Scaling and elevation in River Networks. Water Resour. Res. 25 (9), 2037–2051.

Tarboton, D.G., Bras, R.L., Rodriguez-Iturbe, I., 1991. On the extraction of channel networks from digital elevation data. Hydrological Processes 5 (1), 81–100.

Tarboton, D.G., 1997. A new method for the determination of flow directions and upslope areas in grid digital elevation models. Water Resour. Res. 33 (2), 309–319. https://doi.org/10.1029/96WR03137.

Tarboton, D. G., 2013. TauDEM 5.1 Guide to using the taudem command line functions. http://hydrology.usu.edu/taudem/taudem5/TauDEM51CommandLineGuide.pdf.

Yang, C.T., 1976. Minimum Unit Stream Power and Fluvial Hydraulics. Journal of the Hydraulics Division 102 (7), 919–934.

Zehe, E., Loritz, R., Edery, Y., Berkowitz, B., 2021. Preferential pathways for fluid and solutes in heterogeneous groundwater systems: self-Organization, entropy, work. Hydrol. Earth Syst. Sci. 25, 5337–5353. https://doi.org/10.5194/hess-25-5337-2021.

Zehe, E., Blume, T., Blöschl, G., 2010. The principle of 'maximum energy dissipation': a novel thermodynamic perspective on rapid water flow in connected soil structures. Phil. Trans. R. Soc. B 365 (1545), 1377–1386.

Zehe, E., Ehret, U., Blume, T., Kleidon, A., Scherer, U., Westhoff, M., 2013. A thermodynamic approach to link self-organization, preferential flow and rainfall–runoff behaviour. Hydrol. Earth Syst. Sci. 17 (11), 4297–4322. https://doi.org/10.5194/hess-17-4297-2013.